Energy Materials

Supplementary Materials

Confined iodine and accelerated redox kinetics enable high-rate Zn-iodine batteries

Fei Sheng[2], Mengxue Jin[2], Hedong Jiang[1,*], Dandan Huang[2], Pingchun Guo[2], Kailin Fu[1], Jiake Li[2], Xueguo Zhao[3], Hua Zhu[4], Yanxiang Wang[2,*]

[1]School of Energy Science and Engineering, Jingdezhen Ceramic University, Jingdezhen 333403, Jiangxi, China.

[2]School of Materials Science and Engineering, Jingdezhen Ceramic University, Jingdezhen 333403, Jiangxi, China.

[3]National Engineering Research Center for Domestic & Building Ceramics, Jingdezhen 333403, Jiangxi, China.

[4]School of Mechanical and Electrical Engineering, Jingdezhen Ceramic University, Jingdezhen 333403, Jiangxi, China.

[*]**Correspondence to:** Dr. Hedong Jiang, School of Energy Science and Engineering, Jingdezhen Ceramic University, Jingdezhen 333403, Jiangxi, China. E-mail: 201003@jcu.edu.cn; Prof. Yanxiang Wang, School of Materials Science and Engineering, Jingdezhen Ceramic University, Jingdezhen 333403, Jiangxi, China. E-mail: wangyanxiang@jcu.edu.cn

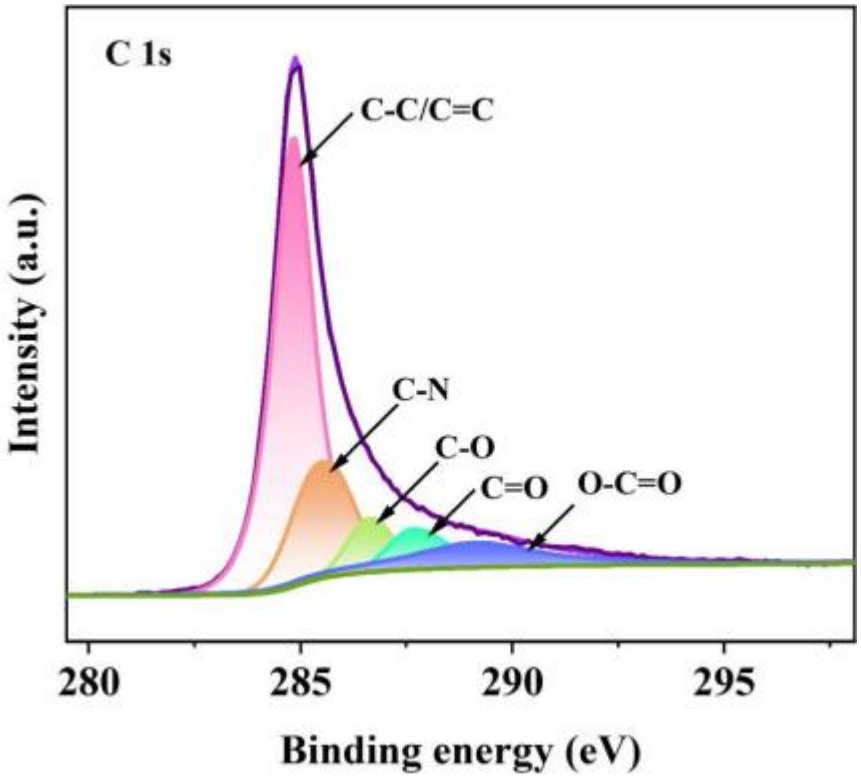

Supplementary Figure 1. C 1s spectrum of RGO-3.

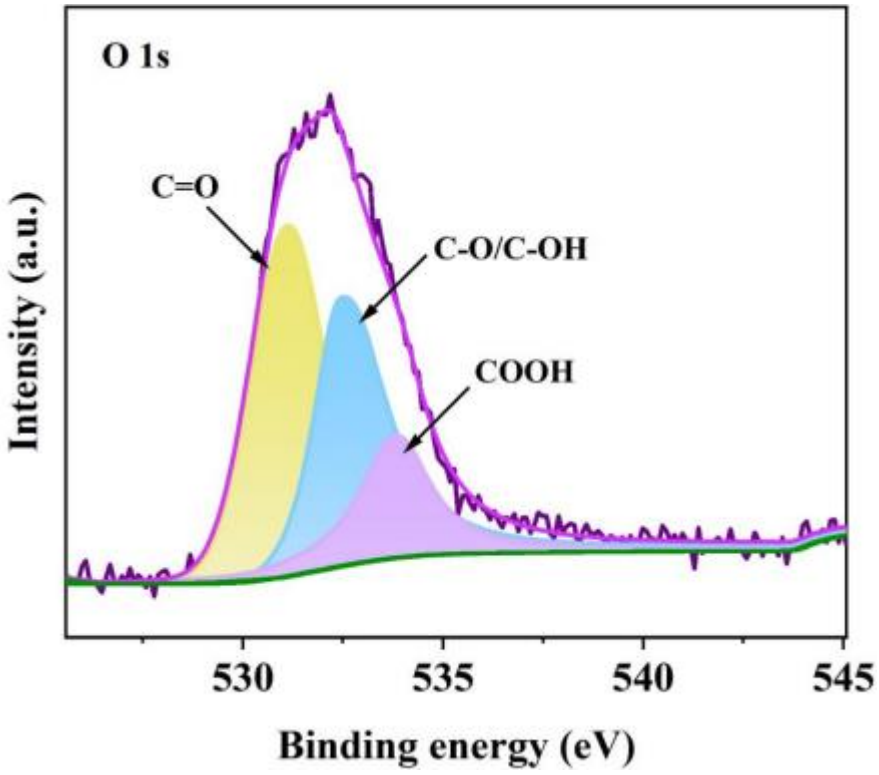

Supplementary Figure 2. O 1s spectrum of RGO-3.

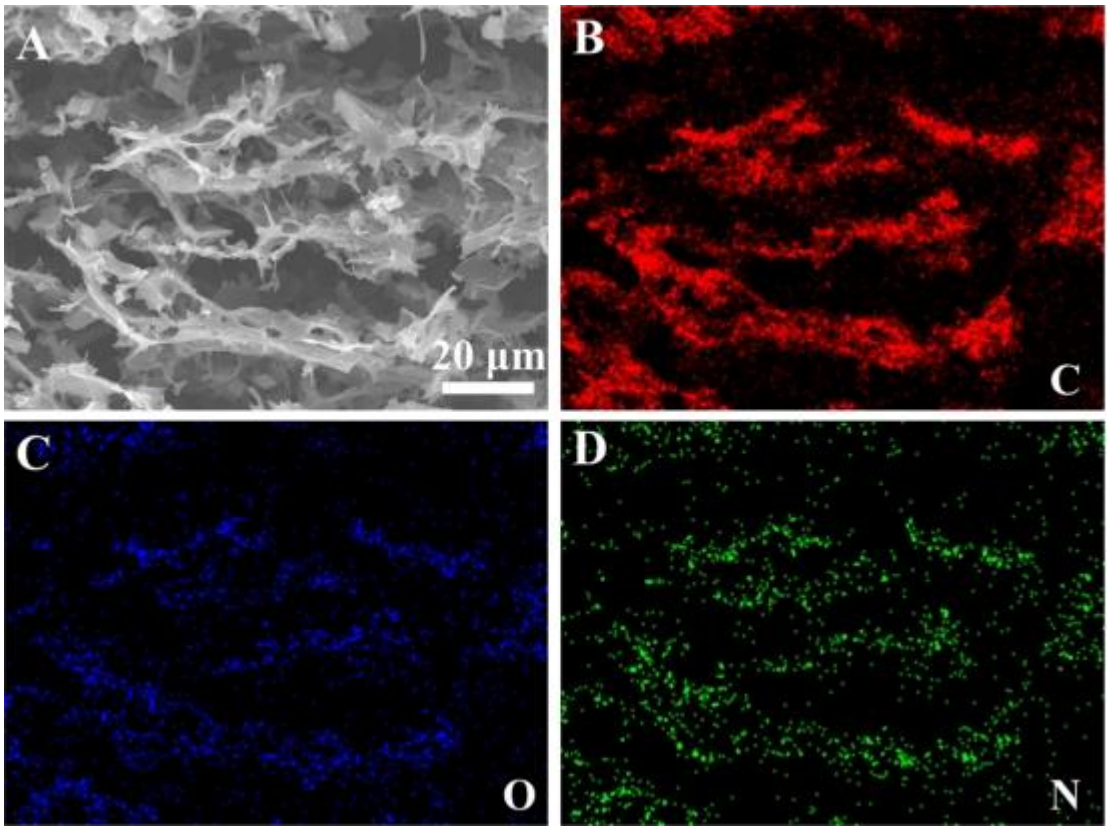

Supplementary Figure 3. (A) SEM image of the RGO-3 section; corresponding elemental mapping of RGO-3: (B) C, (C) O and (D) N.

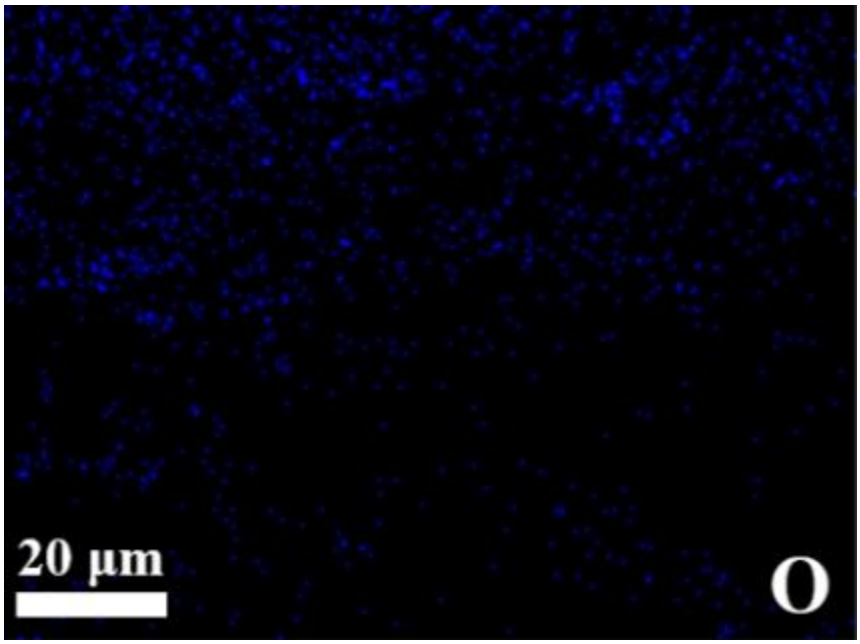

Supplementary Figure 4. Elemental mapping of O in I_2@RGO-3.

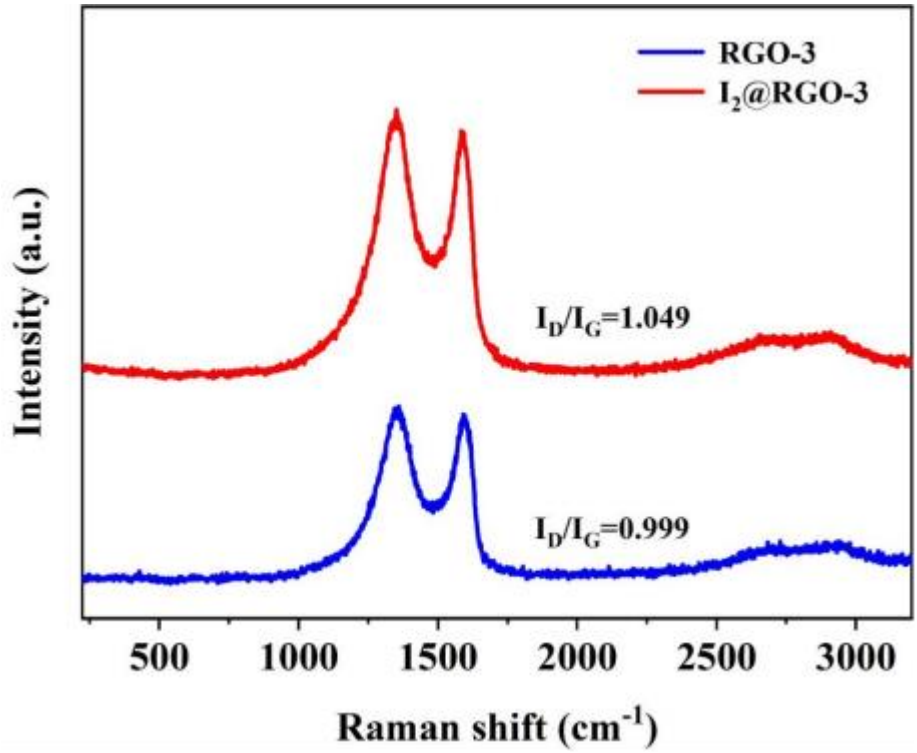

Supplementary Figure 5. Raman spectrum of I_2@RGO-3 and RGO-3.

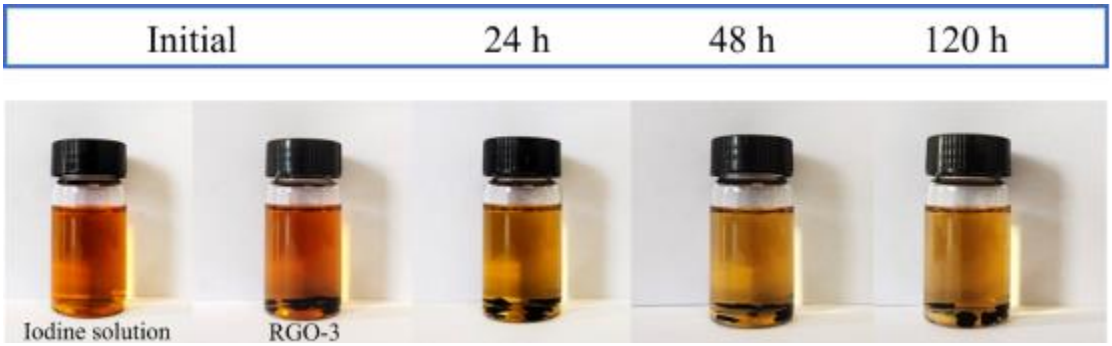

Supplementary Figure 6. Optical images of RGO-3 recorded at different immersion times during iodine adsorption in saturated iodine solution. (Images taken by the authors)

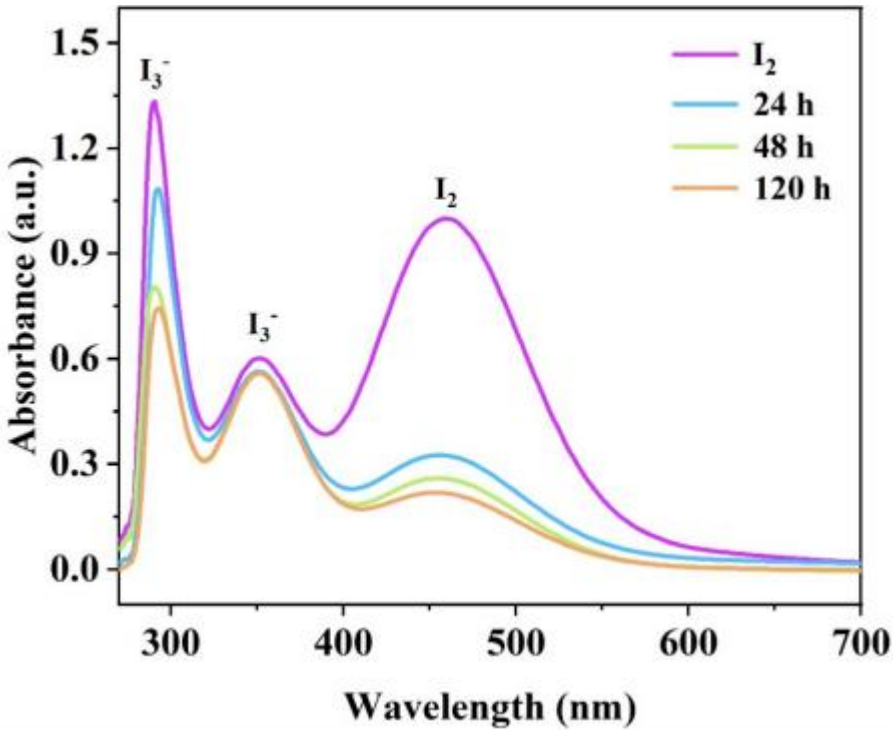

Supplementary Figure 7. UV-vis absorption spectra of the residual iodine solutions after adsorption by RGO-3 for different durations.

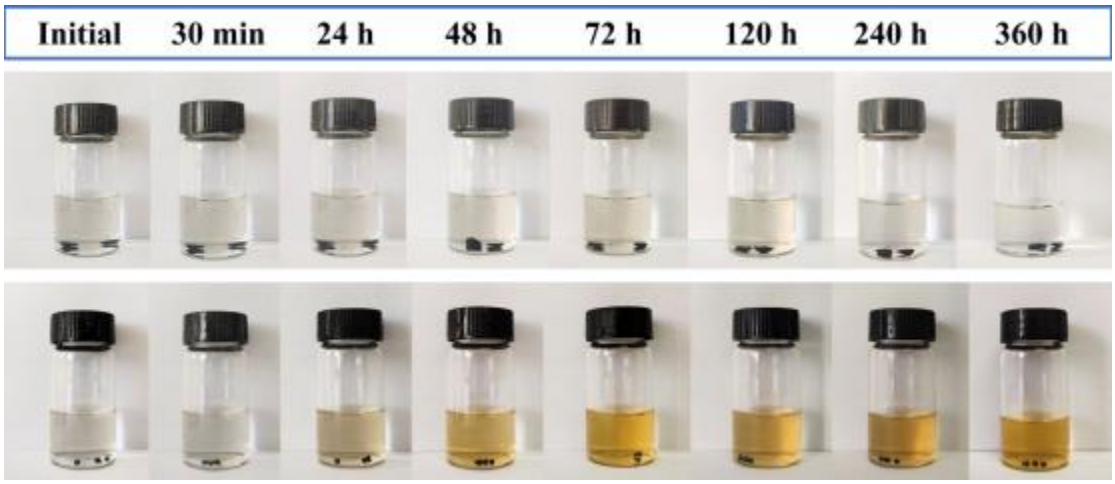

Supplementary Figure 8. Optical photographs showing the color evolution of electrolytes containing I_2@RGO-3 and pure I_2 over 360 h of immersion. (Photographs taken by the authors)

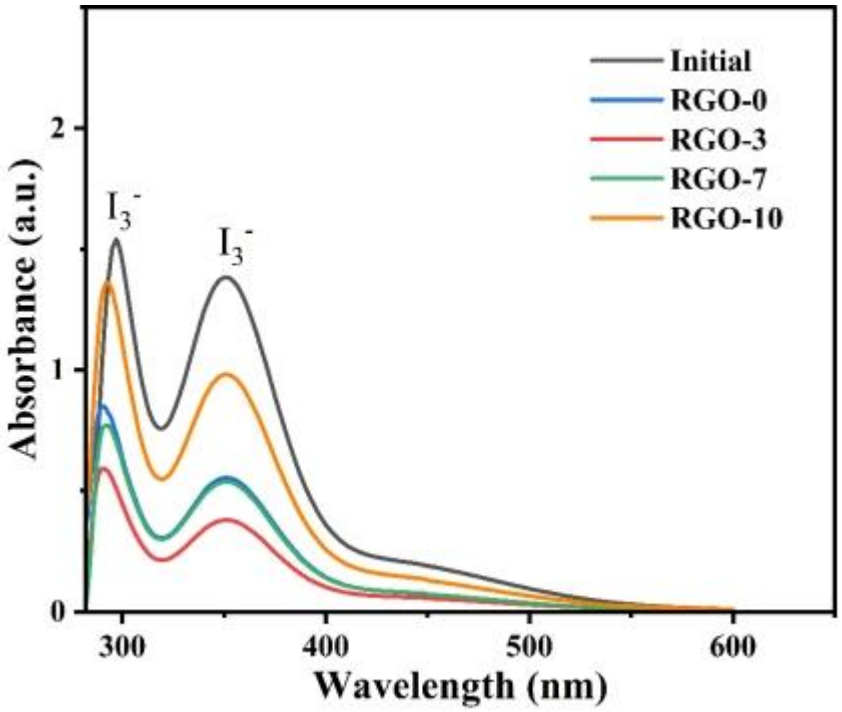

Supplementary Figure 9. UV-vis absorption spectra of the initial triiodide solution and the residual solutions after adsorption with RGO-0, RGO-3, RGO-7, and RGO-10 samples for 12 h.

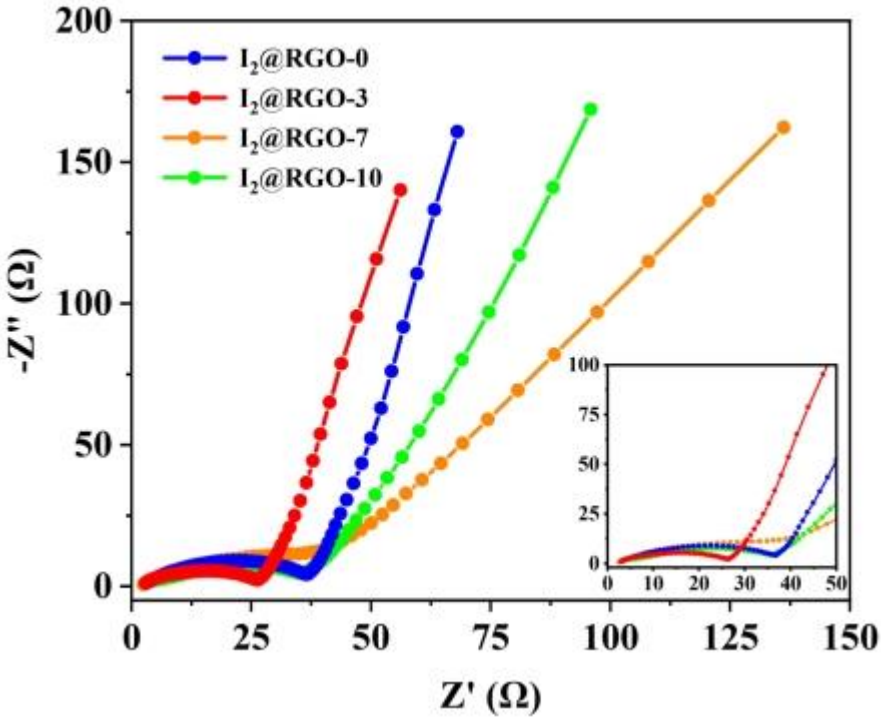

Supplementary Figure 10. Nyquist plots of I_2@RGO-0, I_2@RGO-3, I_2@RGO-7, and I_2@RGO-10 electrodes.

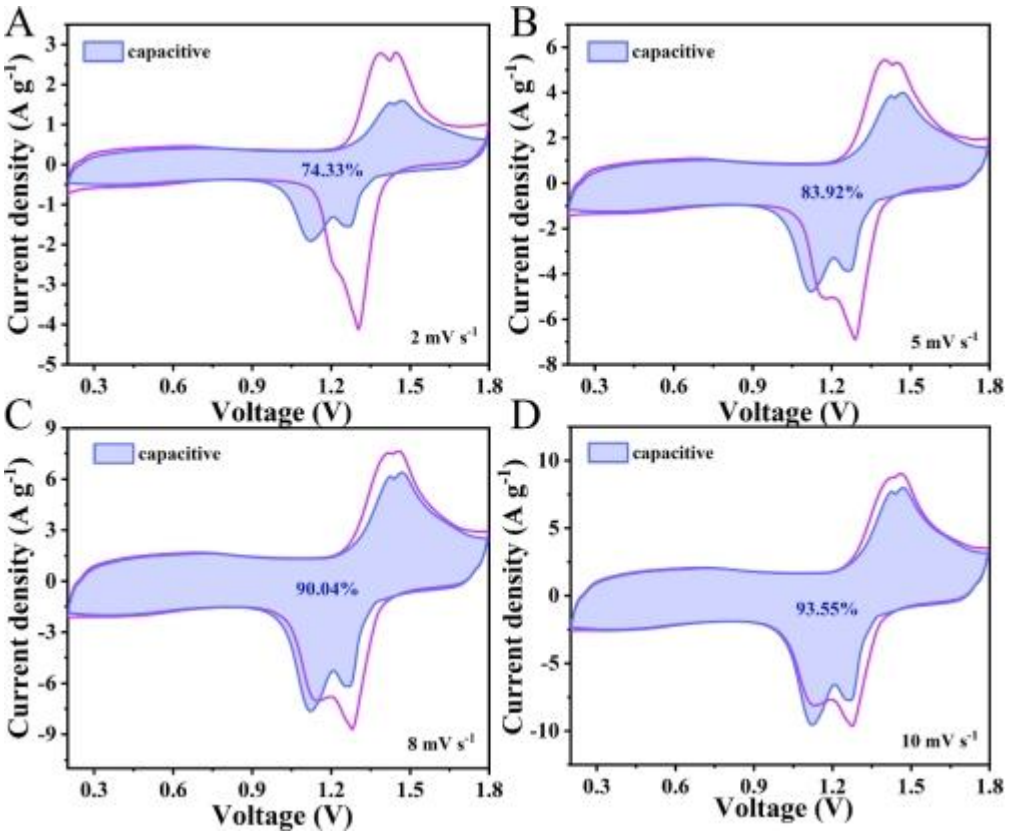

Supplementary Figure 11. Capacitive contribution (blue shaded area) of the electrode at different scan rates: (A) 2 mV s^{-1}, (B) 5 mV s^{-1}, (C) 8 mV s^{-1}, and (D) 10 mV s^{-1}. The percentages indicate the capacitive contribution ratios.

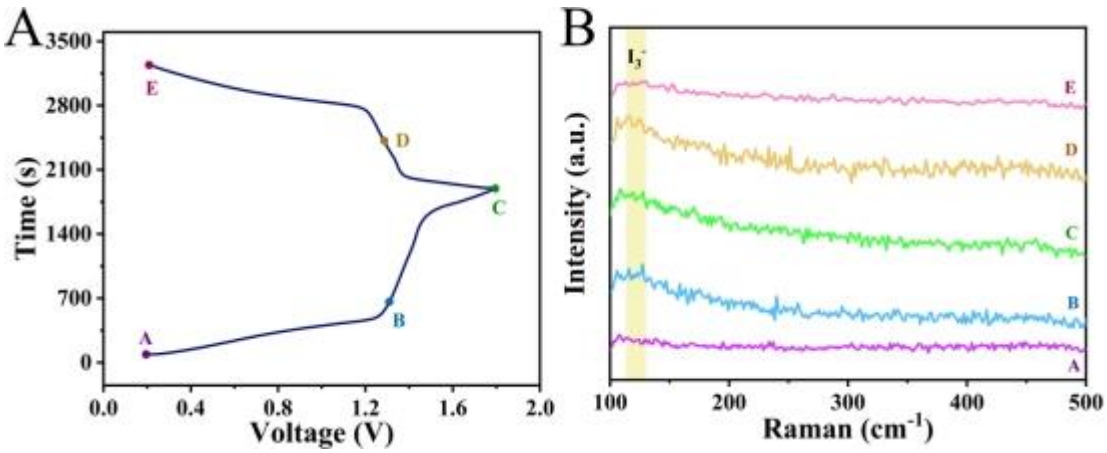

Supplementary Figure 12. (A) GCD curve of I_2@RGO-3//Zn with five distinct points; (B) Ex situ Raman spectra of I_2@RGO-3//Zn at various distinct points.

Ex-situ Raman tests were performed on the I_2@RGO-3 electrode at various marked points on the charging and discharging curves (from point A to point E) to study the

energy storage mechanism of iodine in the ZIB during charging and discharging. At 0.2 V, the I_3^- characteristic peak cannot be detected at point A. As the battery charges to 1.3 V, the I_3^- characteristic peak becomes more obvious at point B, and the intensity of the I_3^- characteristic peak weakens at 1.8 V (point C). This evolution is consistent with the oxidation of I^- through soluble polyiodide intermediates such as I_3^- toward I_2 during charging. During the subsequent discharge process, the reverse evolution was observed: the I_3^- signal became more pronounced at 1.3 V (point D) and gradually weakened to nearly undetectable at 0.2 V (point E), corresponding to the reduction pathway of $I_2 \rightarrow I_3^- \rightarrow I^-$.

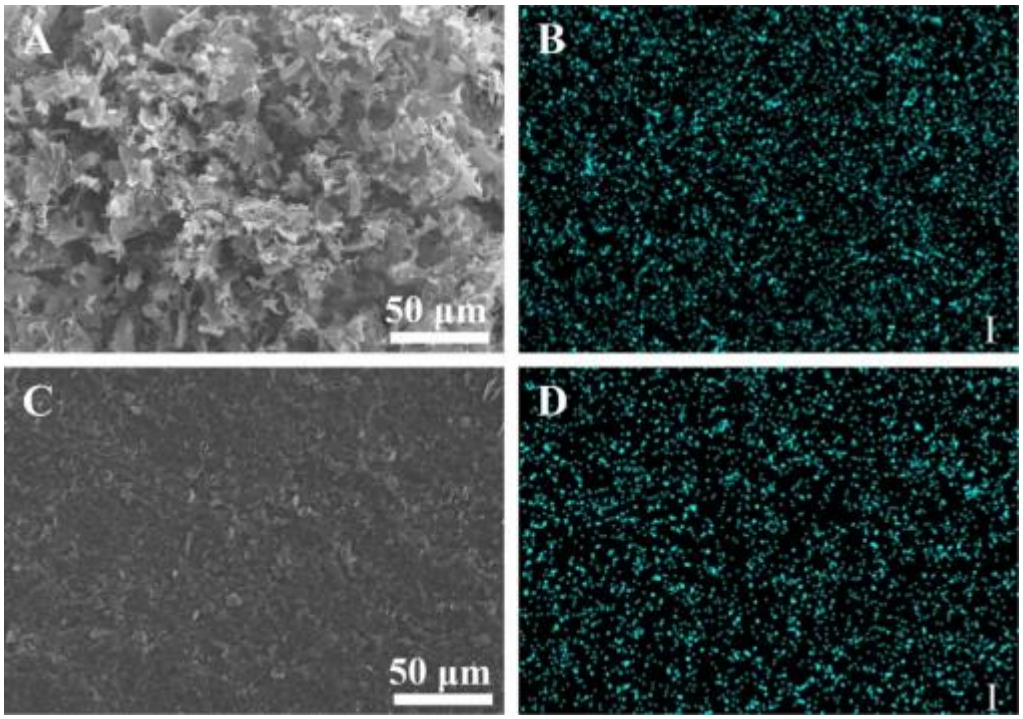

Supplementary Figure 13. SEM images of the I_2@RGO-3 cathode surface and the corresponding I elemental mapping images: (A and B) before cycling; (C and D) after cycling.

Supplementary Table 1. Physical parameters of the I_2@RGO composite electrodes. The data include electrode area, thickness, iodine loading, and zinc anode thickness

Electrode type	area (cm^2)	Thickness (μm)	iodine loading (mg cm^{-2})	Zn thickness (μm)
I_2@RGO-0	≈0.36	285±11	1.78	80
I_2@RGO-3	≈0.25	189±11	4.64	80
I_2@RGO-7	≈0.25	59±6	4.6	80
I_2@RGO-10	≈0.56	49±2	1.25	80

Supplementary Table 2. Comparison of rate performance between I_2@RGO-3 and previously reported iodine-based electrodes

Material	Current density (A g^{-1})	Current-density increase factor	Retention rate (%)	Ref.
This work	0.5~20	40	64.17	
ACop@C/I_2	0.1~5	50	51.7	47
I_2/OSTC	1~3	3	94	48
PTCC900@I_2	0.1~5	50	61.6	49
CMK-3@I_2	0.2~5	25	77.1	50
G/PVP@ZnI_2	0.2~5	25	66.4	51
Starch/I_2	0.2~10	50	37.9	52
mPEDOT:PSS/I_2	0.2~2	10	57.6	53
G-Starch	0.1~2	20	63.8	54
I_2@CCTF-TPMB	0.2~5	25	65	55
PANI-I_2	0.3~2.4	8	48.4	56